Vision Research 158 (2019) 90–99

Contents lists available at ScienceDirect

Vision Research

journal homepage: www.elsevier.com/locate/visres

Evaluating seasonal changes of cone photoreceptor structure in the 13-lined ground squirrel

Benjamin S. Sajdak[a], Alexander E. Salmon[a], Katie M. Litts[b], Clive Wells[c], Kenneth P. Allen[d,e], Alfredo Dubra[f], Dana K. Merriman[g], Joseph Carroll[a,b,h,*]

[a] Cell Biology, Neurobiology, and Anatomy, Medical College of Wisconsin, Milwaukee, WI, USA
[b] Ophthalmology & Visual Sciences, Medical College of Wisconsin, Milwaukee, WI, USA
[c] Microbiology and Molecular Genetics, Medical College of Wisconsin, Milwaukee, WI, USA
[d] Biomedical Resource Center, Medical College of Wisconsin, Milwaukee, WI, USA
[e] Microbiology and Immunology, Medical College of Wisconsin, Milwaukee, WI, USA
[f] Ophthalmology, Stanford University, Stanford, CA, USA
[g] Biology, University of Wisconsin Oshkosh, Oshkosh, WI, USA
[h] Biophysics, Medical College of Wisconsin, Milwaukee, WI, USA

ARTICLE INFO

Keywords:
Cone photoreceptors
Ground squirrel
Adaptive optics
Hibernation
Electron microscopy

ABSTRACT

Cone photoreceptors of the 13-lined ground squirrel (13-LGS) undergo reversible structural changes during hibernation, including cone outer segment disc degeneration and inner segment mitochondria depletion. Here, we evaluated cone structure with adaptive optics scanning light ophthalmoscopy (AOSLO) before, during, and after hibernation. Also, intra-animal comparisons of cone structure were made at distinct physiological states (pre-hibernation, torpor, interbout euthermia, and post-hibernation) with AOSLO and transmission electron microscopy. Our results indicate that the 13-LGS cone mosaic is only transiently affected by structural remodeling during hibernation. Outer segment remodeling starts during torpid states during a period of fall transition in room temperature, with more severe structural changes during bouts of torpor in cold temperature. Cones return to euthermic-like structure during brief periods of interbout euthermia and recover normal waveguiding properties as soon as 24 h post-hibernation. Cone structure is visible with split-detector AOSLO throughout hibernation, providing evidence that intact outer segments are not necessary to visualize cones with this technique. Despite the changes to cone structure during hibernation, cone density and packing remained unchanged throughout the seasonal cycle. Pairing non-invasive imaging with ultrastructural assessment may provide insight to the biological origins of cone photoreceptor signals observed with AOSLO.

1. Introduction

The retina is a uniquely accessible neural tissue, and technological advancements allowing *in vivo* assessment of cellular structures *en face* have come a long way since initial success of viewing the cone mosaic using the eye's natural optics (Jagger, 1985; Land & Snyder, 1985; Miller, Williams, Morris, & Liang, 1996; Wade & Fitzke, 1998). Correction of the eye's monochromatic aberrations with adaptive optics scanning light ophthalmoscopy (AOSLO) results in nearly diffraction-limited imaging of the cone mosaic (Roorda et al., 2002). While cone disorders have been extensively studied non-invasively in patients using AOSLO (Roorda & Duncan, 2015), biological interpretation of cone structure seen with this instrumentation is not well understood. With confocal AOSLO imaging in visually normal human subjects, cones appear as bright or reflective spots. This reflective appearance is often linked to the cone's ability to guide light back to the system's detector (i.e., "waveguiding"), and this reflectivity varies over time (Pallikaris, Williams, & Hofer, 2003). In patients with cone dystrophies, cones often have reduced or absent waveguiding (Carroll, Choi, & Williams, 2008; Song et al., 2015; Sun et al., 2016), though some patients will show spontaneous recovery of cone reflectivity over time (Horton, Parker, Botelho, & Duncan, 2015). Some cones can have measurable function in regions of abnormal or absent reflectivity (Bruce et al., 2015; Tu et al., 2017; Wang et al., 2015), suggesting that non-reflective cones may still have some light-capturing structure to provide this function.

The alternative modality of non-confocal split-detection AOSLO can reveal residual cone structure that otherwise appears dim or absent when using only confocal AOSLO (Scoles et al., 2014). Combining

* Corresponding author at: Department of Ophthalmology & Visual Sciences, Medical College of Wisconsin, 925 N 87th St, Milwaukee, WI 53226-0509, USA.
E-mail address: jcarroll@mcw.edu (J. Carroll).

https://doi.org/10.1016/j.visres.2019.02.009
Received 9 November 2018; Received in revised form 21 January 2019; Accepted 24 February 2019
Available online 07 March 2019
0042-6989/

confocal AOSLO with split-detection AOSLO to reveal reflective and non-reflective cone structure simultaneously makes this method potentially capable of assessing living cone structure and function at a sub-cellular level. While cone structure seen with split-detection AOSLO is thought to correspond to the cell's inner segment due to a comparable diameter when examined with histology (Scoles et al., 2014), it is not known whether an intact outer segment is required for the visualization of cones with split-detection AOSLO. Further, it is not known how changes to cone outer segments alter confocal AOSLO reflectivity. Insight into these questions can be gained from the use of cone-rich animal models. For example, ground squirrel evolution has provided us a natural model of reversible cone degeneration with which to address the interpretation of AOSLO images (Merriman, Sajdak, Li, & Jones, 2016).

The 13-lined ground squirrel (13-LGS; *Ictidomys tridecemlineatus*) has a cone-dominant retina that can be readily imaged with AOSLO (Sajdak et al., 2016). These diurnal rodents hibernate for 5–8 months starting in the fall. Hibernation is a regulated adaptation of metabolic flexibility used by some mammals to survive lengthy periods of limited resources. This phenomenon is known for its drastic state of suppressed metabolic activity accompanied by whole-body hypothermia, known as torpor, that lasts several days (Andrews, 2007; Staples, 2016). Ground squirrel hibernation is not a single continuous period of metabolic suppression and cold body temperature; instead, it is a cycle that includes a series of torpor bouts with brief periods of increased metabolism and body temperature back to euthermic levels (Fig. 1). Each 13-LGS prepares for hibernation during a period of fall transition, in which it experiences varying degrees of heterothermy in room temperature (Russell, O'Neill, Epperson, & Martin, 2010). Once introduced to ambient cold (4 °C), each bout of torpor last about 1–2 weeks, interrupted by energetically costly states of interbout euthermia (IBE, also called interbout arousal) that last about 12–24 h (Carey, Andrews, & Martin, 2003; Staples, 2016). Physiological characteristics of torpor in the 13-LGS include reduced body temperature to 2–10 °C (compared to 37 °C in euthermia) and a heart rate as low as 3–10 beats per minute (compared to 200–300 beats per minute in euthermia) (Andrews, 2007). The hibernation cycle can be reliably monitored within laboratory conditions (Merriman, Lahvis, Jooss, Gesicki, & Schill, 2012), making it an appealing natural state during which to study tissue resilience to prolonged cold environments and drastically decreased metabolism. While hibernation is commonly used to study unique adaptations in heart, kidney, skeletal muscle, and adipose tissue (Staples, 2016), it is less commonly used to study adaptations of the visual system (Merriman et al., 2016).

During hibernation, 13-LGS cones imaged with transmission electron microscopy (TEM) have been shown to exhibit shortened (potentially absent) outer segments and depleted inner segment mitochondria (Kuwabara, 1975; Remé & Young, 1977); see (Merriman et al., 2016) for a complete review of retinal remodeling in the ground squirrel. Upon arousal from hibernation in spring, these cone changes reverse. This type of natural cone remodeling may be informative as to the origin of signals within AOSLO imagery. Here, we used three different AOSLO modalities (confocal, split-detection, and dark-field) to longitudinally evaluate 13-LGS cone structure throughout the hibernation cycle and provide intra-animal comparisons of AOSLO and TEM at distinct physiological states.

2. Materials and methods

2.1. Animal subjects and hibernation monitoring

The experimental procedures described were approved by the Institutional Animal Care and Use Committee of the Medical College of Wisconsin (AUA00005654) and were in accordance with the ARVO Statement for the Use of Animals in Ophthalmic and Vision Research.

Eight female and seven male 13-LGS were obtained from the University of Wisconsin Oshkosh Squirrel Colony for use in this study at the Medical College of Wisconsin. Animals were used from September to July during the 2016–2017 hibernation season, and from November to February during the 2017–2018 hibernation season. Animals used during the fall transition were kept in room temperature between the months of September and November and examined during a torpid state (called "fall transition" hereafter, Fig. 1). Animals used during winter torpor (called "torpor" hereafter) were placed in a dark 4 °C hibernaculum (True Manufacturing, O'Fallon, MO, USA) without food or water, and allowed to hibernate for over 2 months before they were used for the study. Animals in the hibernaculum were checked daily for activity remotely by infrared camera (Axis Communications, Lund, Sweden), in a strategy inspired by the traditional "sawdust method" (Pengelley & Fisher, 1961) that uses the movement of sawdust placed on the back of the ground squirrel to detect activity. With our method, an image was captured of 13-LGS nests every day by the Axis Companion software (Axis Communications, Lund, Sweden). Bedding that moved from the previous day was recorded as a period of IBE. All animals used for IBE assessments were inactive (and presumably in continual torpor) for greater than 1 week. Additional daily checks were performed briefly (~2 mins) by animal care staff to check for cage condensation (indicating euthermic activity). Squirrels were removed from the hibernaculum if euthermic activity persisted for > 48 h.

Animals in fall transition or summer euthermia were kept on a natural photoperiod with light adjusted every 2 weeks to replicate day lengths in southern Wisconsin, while animals in winter torpor and IBE were kept in the constantly dark 4 °C hibernaculum. Care was taken during the transport of torpid fall transition and winter animals (from the animal room or hibernaculum, respectively) to the procedural suite or room temperature housing, to limit disturbance and avoid any increase in arousal speed that is known to occur with physical stimulation (Christian et al., 2014). To verify physiological state, squirrel body temperature was measured by a FLIR E60 thermal imaging camera (FLIR Systems, Inc., Wilsonville, OR, USA) and/or by subcutaneous IPTT-300 temperature transponders (Bio Medic Data Systems, Seaford, DE, USA). To assess retinas during post-hibernation time points (1.5 h, 24 h, 72 h, or 1 week), squirrels were removed from the hibernaculum and placed in room temperature in a well-lit room where they aroused to euthermia. All imaging and euthanasia were performed between the hours of 10 AM and 6 PM.

2.2. Adaptive optics scanning light ophthalmoscopy (AOSLO)

Five 13-LGS were imaged longitudinally before, during, and after hibernation with three simultaneous AOSLO modalities (confocal, non-confocal split detection, and non-confocal dark-field). Ten 13-LGS were imaged with AOSLO at a single time-point, then subsequently used for histology. Prior to imaging, squirrels in fall transition, IBE, euthermic, and post-hibernating physiological states were anesthetized with inhaled isoflurane (up to 5% for induction in a chamber, 0.5–4% maintenance via mask delivery) in 1 L/min oxygen flow. Torpid squirrels were prepared for imaging as previously described (Sajdak et al., 2018), not requiring induction and using a 2% maintenance dose of inhaled isoflurane.

The imaged eye was first dilated and cyclopleged with phenylephrine hydrochloride (2.5%) and tropicamide (1%), and the lids were held open with a pediatric ocular speculum. Wetting drops (Saline and/or Systane (Alcon, Fort Worth, TX, USA)) were applied every 1 to 2 min throughout the AOSLO examinations. Images of the cone mosaic[1] were

[1] Rod and cone photoreceptors are similar in size in the 13-LGS (von Schantz, Szél, van Veen, & Farber, 1994), and therefore difficult to distinguish with AOSLO. The superior retinal regions imaged in this study are reported to have less than 10% rod photoreceptors (Kryger, Galli-Resta, Jacobs, & Reese, 1998), so we will refer to the AOSLO images as images of the cone mosaic.

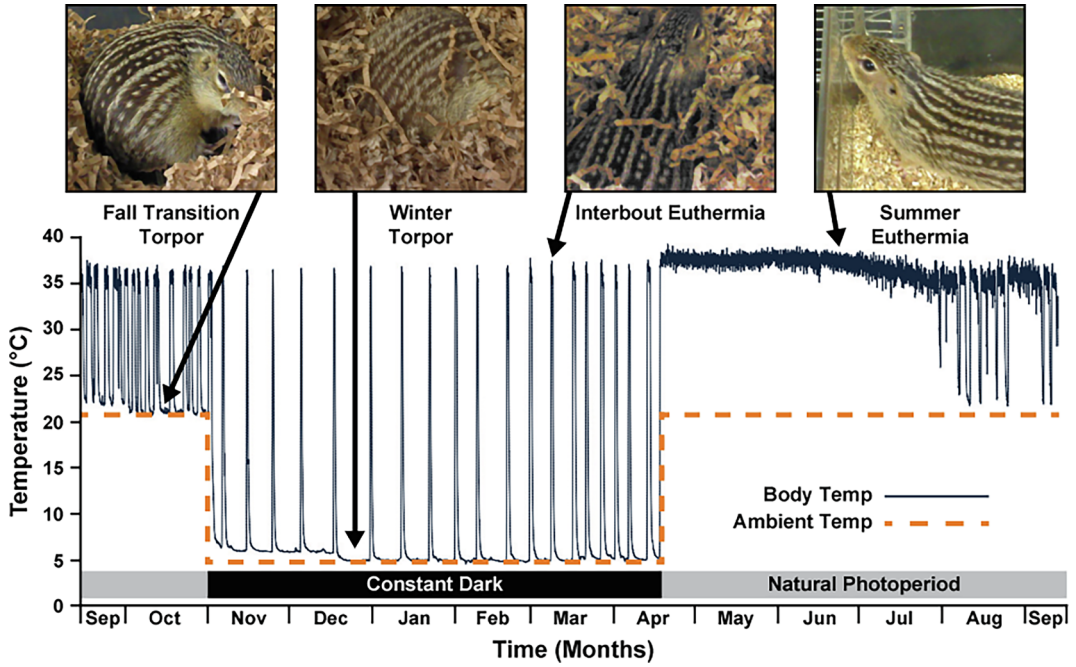

Fig. 1. Illustration of physiological states of the 13-lined ground squirrel seasonal cycle. Body temperature (solid line) of 1 animal measured in two ambient temperature environments (dashed line; 4 °C starting November, and 21 °C starting in April). Fall transition varies in onset and frequency between animals (Russell et al., 2010), but often includes periodic reductions in body temperature and metabolic activity while in room temperature (21 °C). Periods of interbout euthermia occur every ~1–2 weeks during hibernation. This figure was adapted with permission from (Cooper et al., 2016; Vermillion, Jagtap, Johnson, Griffin, & Andrews, 2015). Copyright (2015) American Chemical Society. Body temperature was not continuously measured in our study.

acquired using a custom AOSLO (Dubra & Sulai, 2011) modified for a 4.5 mm pupil diameter (approximate size of the dilated 13-LGS pupil). Confocal and non-confocal AOSLO videos of the superior retina were captured as previously described in this species (Sajdak et al., 2016). The split-detection AOSLO signal is generated from the subtraction of the two non-confocal detector intensities divided by their sum at every pixel, while the dark-field AOSLO signal is generated by averaging the two non-confocal detector intensities at every pixel (Scoles, Sulai, & Dubra, 2013).

Image sequences were first collected at the horizontal optic nerve head, which has a unique pattern of pores that serve as a "roadmap" for repeated imaging of the same retinal location. Sinusoidal distortion inherent in our scanning system was estimated by imaging a Ronchi grating of known spacing, then corrected by resampling the video frames over a grid of equally-spaced pixels. The scale of the AOSLO images was determined by calculating the degrees per pixel in the re-sampled image of the Ronchi grating. Reference frames were automatically selected (Salmon et al., 2017), then image sequences were automatically registered and averaged to improve signal-to-noise ratio (Dubra & Harvey, 2010). The resulting images were automatically montaged with custom software employing a semi-automated SIFT-feature matching algorithm (Chen et al., 2016).

To examine changes in the cone mosaic throughout hibernation, AOSLO montages from each time point were scaled and manually aligned using Photoshop CS6 (Adobe, San Jose, CA, USA) to the largest montage using optic nerve pores and vessels, then cropped to the overlapping region and aligned again to a common 0.5 × 0.5° region of photoreceptors. Individual cells were semi-automatically identified from the split-detector images using the "adaptive filtering and local detection" algorithm (Cunefare et al., 2016). Cone density and Voronoi pattern were then analyzed using custom software (Cooper, Wilk, Tarima, & Carroll, 2016).

2.3. Transmission electron microscopy (TEM)

Ten 13-LGS imaged with AOSLO at single time-points throughout the hibernation cycle were euthanized immediately after imaging (within 2 min of final image capture) by decapitation under isoflurane anesthesia. Both eyes were enucleated and the whole globe was immersion-fixed overnight in 2% paraformaldehyde plus 2% glutaraldehyde in 0.1 M sodium cacodylate buffer. Following fixation, the eyes were rinsed 3 × 5 min in 0.1 M cacodylate buffer.

The eyes used for TEM then had the cornea and lens removed, and sample regions were dissected from the superior retina (the location imaged with AOSLO) of the eyecup. The samples were post-fixed in 1% osmium tetroxide followed by dehydration in a graded methanol series. Subsequently, the samples were infused with acetonitrile before infiltration with Embed 812 (Electron Microscopy Sciences, Hatfield, PA, USA) and cured overnight in a 60 °C oven. Then 0.5 μm sections were cut on an Ultracut E microtome (Reichert-Jung/Leica Microsystems, Wetzlar, Germany) and stained with 1% toluidine blue to ensure the sample was block-faced in the correct orientation. Both vertical cross-sections and horizontal *en face* sections were prepared from each eye imaged with AOSLO (and several contralateral eyes to serve as fixation controls). For TEM, 70 nm sections were cut using a PowerTome PT-XL ultramicrotome (RMC Boeckeler, Tucson, AS, USA), and stained with uranyl acetate and lead citrate. Imaging was performed on an H-600 transmission electron microscope (Hitachi High Technologies, Schaumburg, IL, USA). Five cone inner segment ellipsoids and their mitochondria were manually segmented from *en face* TEM images from each animal (n = 10) using the Track2EM FIJI plugin (Cardona et al., 2012).

2.4. Serial block-face scanning electron microscopy (SEM) reconstruction

Two additional 13-LGS (one euthermic and one torpid) were used for scanning electron microscopy (SEM) without prior AOSLO. Fixed retina samples from the visual streak of each 13-LGS were sent in 0.1 M

cacodylate buffer to Renovo Neural Inc. (Cleveland, OH, USA) for serial block-face imaging SEM. There, retinas were washed, then stained with 1% tannic acid for 30 min and then incubated successively with osmium ferrocyanide, thiocarbohydrazide, osmium tetroxide, and lead aspartate, as previously described (Deerinck et al., 2010; Mukherjee et al., 2016). Tissues were dehydrated and embedded in Epon resin (Electron Microscopy Sciences, Hatfield, PA, USA). Trimmed samples were imaged using a ThermoFisher Volume Scope in-chamber ultramicrotome system (ThermoFisher Scientific, Hillsboro, OR, USA) on a Teneo SEM platform using the T1 detector. On both systems, stacks of digital images were acquired at 7.0 nm/pixel resolution at 2.2 kV, using 65 nm steps; these are standard setting that produce images comparable to those from TEM systems. Each resulting serial image stack contained ~500 images (~33 μm deep, 49 × 49 μm wide). For analysis, images were scaled, and sub-stacks generated and aligned using ImageJ software with the FIJI plugin suite (Schindelin et al., 2012). Outer segment discs and mitochondria were manually segmented in 3 euthermic and 3 torpid 13-LGS cones using the Track2EM plugin (Cardona et al., 2012).

2.5. Statistical analysis

All statistical tests were performed using Prism version 7.04 (GraphPad, La Jolla, CA, USA). D-Agostino & Pearson tests were performed to test the normality of each data set and determine each statistical method. For longitudinal assessment of cone density in the same animal across 5 different physiological states, a one-way ANOVA with repeated measures was performed. For comparing cone density in two physiological states, before and after torpor, using 5 animals, a Tukey's multiple comparisons test was performed. For comparing mitochondria area fraction in TEM images, 5 cones measured from 2 animals were grouped for 5 distinct physiological states, and a one-way between groups ANOVA was performed. Measurements of outer segment volume, mitochondrial volume, and mitochondrial number from SEM image volumes were collected from 3 cones for 2 physiological states, and each did not pass the normality test, so Mann-Whitney or Kolmogorov-Smirnov tests were performed. Significance values are $^{**}P < 0.01$; $^{***}P < 0.001$; $^{****}P < 0.0001$ where relevant.

3. Results

3.1. Longitudinal assessment of cone structure throughout hibernation

To determine how the cone mosaic changes throughout the different physiological states, we used AOSLO to image the same retinal region in five squirrels in the five distinct physiological states. The cone mosaic was unaffected by hibernation; cone density did not significantly change in longitudinal assessments of the same region ($P = 0.51$, $n = 5$, one-way ANOVA with repeated measures, Fig. 2). Two of the squirrels imaged during torpor had poor image quality, which affected cell identification (Fig. 2). Fig. 3 shows a representative location of 13-LGS retina longitudinally assessed with AOSLO. Average cone density was not significantly different when comparing before (fall transition) and after (24 h post-hibernation) torpor (mean ± SD difference = 5.3 ± 3.5 cells/deg^2, $P = 0.58$, $n = 5$, Tukey's multiple comparisons test), and cell packing was consistent between states as well (Fig. 3).

A very small subset of individual photoreceptors (4 out of ~17,500 visible before hibernation) became progressively undetectable with any of the AOSLO modalities after hibernation. Fig. 3 shows an example of a photoreceptor (presumed cone) that became progressively undetectable by AOSLO after arousal from hibernation. Interestingly, the reflective properties of the photoreceptor were visible with confocal AOSLO at 24 h post-hibernation, and this reflectance was lost 72 h post-hibernation. Residual structure was visible by split-detection and dark-field AOSLO at 72 h post-hibernation. At the euthermic assessment 4 months after hibernation, the residual structure became undetectable in all three AOSLO modalities.

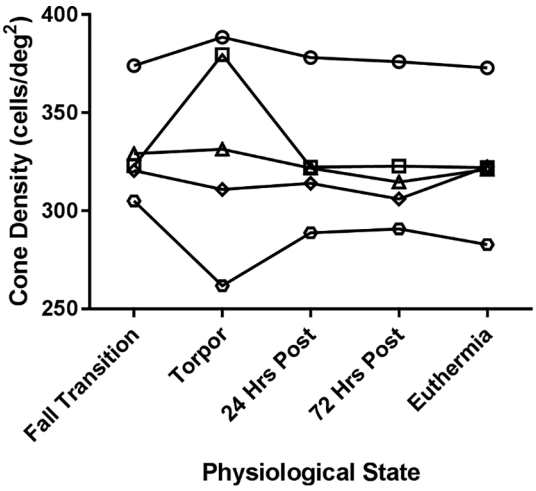

Fig. 2. Longitudinal assessment of cone density, just superior to the optic nerve head, in 5 different animals. Only two cone density measurements (from images captured in torpid animals) appeared to deviate, although cone density did not change significantly ($P = 0.51$, $n = 5$, one-way ANOVA with repeated measures). Density was calculated in degrees, but the y axis can be estimated to range from 25,000 to 40,000 cells/mm^2 when assuming a retinal magnification factor of 100 μm/degree (based on the 7.90 mm axial length of the European ground squirrel (Hughes, 1977)).

3.2. Intra-animal in vivo and ex vivo assessment of photoreceptors throughout hibernation

Fig. 4 shows intra-animal comparisons of the cone mosaic with confocal AOSLO and outer segment structure with TEM. The level of confocal AOSLO signal disruption and outer segment organization were often associated. Confocal AOSLO signal was most disrupted during torpor and 1.5 h after hibernation, and TEM of cones revealed reduced and disorganized outer segment disc structure during these physiological states (Fig. 4). However, cone outer segment disc disruption was also observed during fall transition, without severe disruption in confocal AOSLO (Fig. 4). Further, confocal AOSLO signal and cone structure seem to recover during the brief periods of IBE (Fig. 4), suggesting that outer segment discs recover during these ~12–24 h periods of increased metabolic activity. By 1 week after hibernation, confocal AOSLO signal appeared normal and cone outer segment discs recovered and extended to the distal tips of the cone sheath.

We investigated the relationship between split-detection AOSLO signal and mitochondrial volume using the same regions examined in Fig. 4. Cones were detectable using split-detection AOSLO throughout the seasonal cycle (Fig. 5A), despite the variability in confocal AOSLO signal at the same locations (Fig. 4A). Cone mitochondria visualized by TEM were sparser in pre-hibernation, torpor, and 1.5 h after hibernation, but appeared more abundant during IBE and 1 week post-hibernation (Fig. 5B). To examine this quantitatively, mitochondria were segmented within the inner segment ellipsoid at each physiological state (Fig. 5C–D), revealing significantly increased mitochondrial area fraction (mitochondria area ÷ inner segment ellipsoid area) during IBE relative to all other physiological states (Fig. 5D). While the mitochondrial volume was reduced in fall transition and torpor, and did not recover by 1.5 h after hibernation, cone mitochondria were larger in those two metabolically-suppressed states compared to mitochondria in IBE and 1 week after hibernation (Fig. 5B).

3.3. Cone outer segment and inner segment 3D comparisons in euthermic and torpid retina

We examined outer segment disc and inner segment mitochondrial volumes in cones from one euthermic and one torpid 13-LGS retina

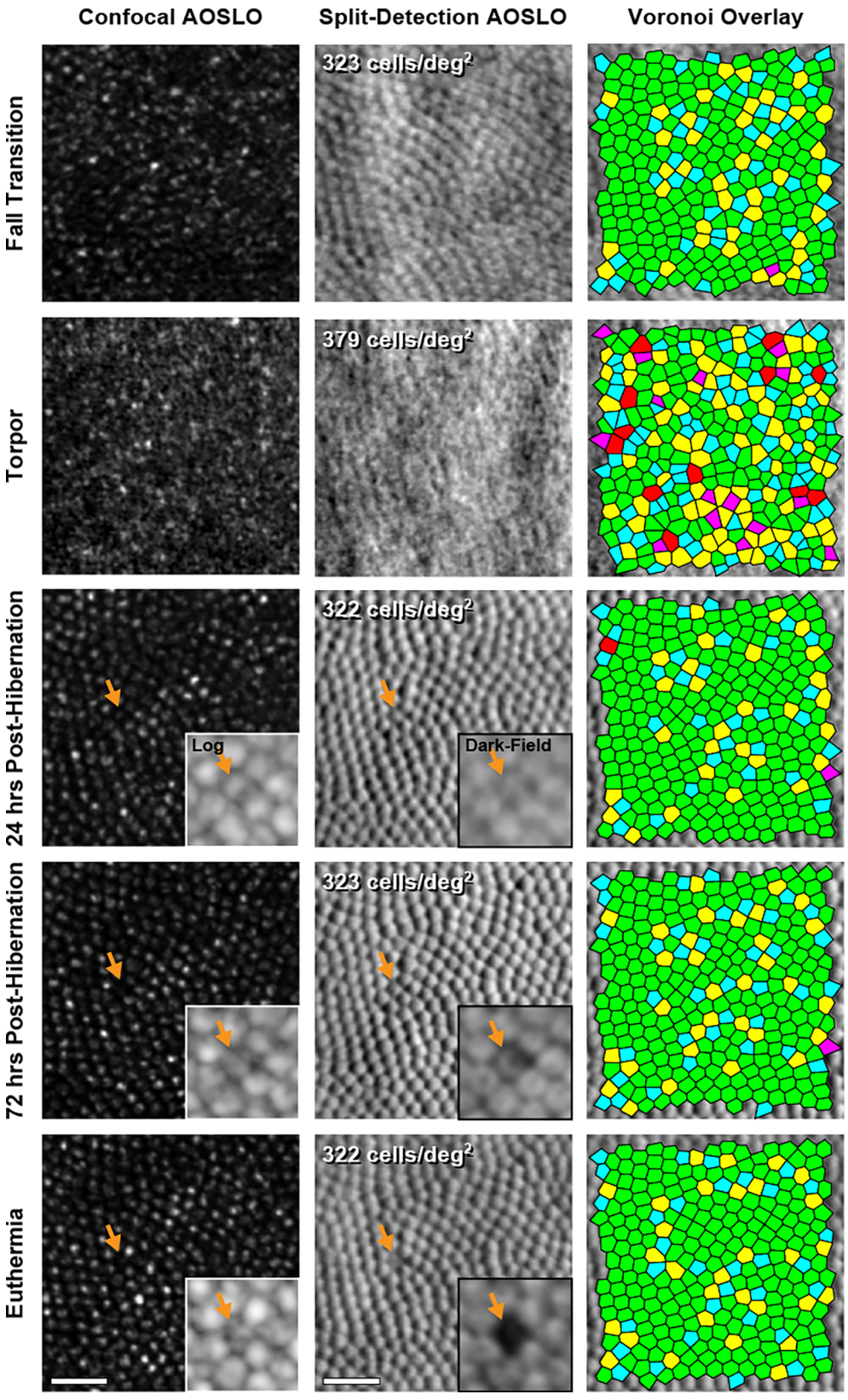

Fig. 3. Longitudinal assessment of the photoreceptor mosaic throughout the 13-LGS seasonal cycle. Photoreceptor reflectivity in confocal AOSLO (left column) is disrupted during a metabolically suppressed state of fall transition, and this disruption increases during torpor. Despite these changes, cone density measured from split-detection AOSLO images (center column) did not change before and after torpor. Rarely, a non-waveguiding photoreceptor will become undetectable by split-detection AOSLO, leaving a gap rather than maintaining residual structure (orange arrows). Insets show close-up images of the cone with progressively extinguished AOSLO signal (confocal inset in log scale; split-detection inset is dark-field). 72 h after hibernation this cone is not reflective, but has residual structure seen with non-confocal AOSLO (split-detection and dark-field). Interestingly, this cone has altered dark-field signal at 72 h, then progresses to undetectable in the euthermic state (4 months after hibernation), creating a gap in the mosaic easily seen with dark-field AOSLO. Voronoi overlays (right column) show that cell packing remained constant before and after torpor (44.1% six-sided cells in torpor, compared to 73.5 ± 3.8% (mean ± SD) six-sided cells in all other physiological states in this animal). Number of sides in Voronoi overlay: pink = 4-sides, blue = 5-sides, green = 6-sides, yellow = 7 sides, red = 8 sides. It is difficult to distinguish structural changes from reduced image quality in the torpid time-point in this example, but structure appeared "euthermic-like" just 24 h after torpor. Scale bars = 20 μm. (For interpretation of the references to colour in this figure legend, the reader is referred to the web version of this article.)

using 3D SEM segmentations. Fig. 6A–B show the 3D SEM segmentations of outer segment discs and inner segment mitochondria bundles used for this analysis. Outer segment disc volume was 30.84 ± 2.72 μm^3 and 24.85 ± 4.25 μm^3 in cones from euthermic and torpid 13-LGS, respectively, supporting outer segment disc reduction seen in other studies, although the outer segment disc reduction was not significant ($P = 0.2$, $n = 3$ cone outer segments each, Mann Whitney test). No completely absent outer segments were seen in any torpid SEM (or TEM) samples in this study, suggesting that while outer segments are indeed variably disrupted, outer segment discs are not commonly eliminated completely within the cone outer segment sheath. Mitochondrial volume was 0.43 ± 0.32 μm^3 (3 cones, $n = 337$

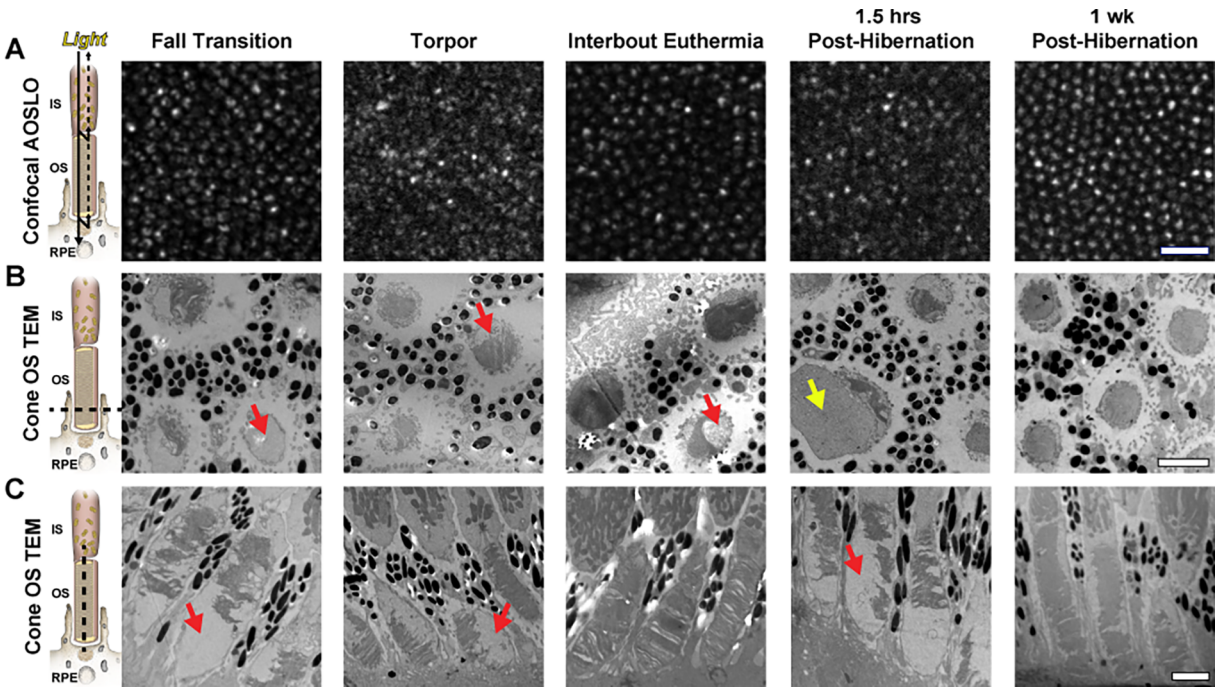

Fig. 4. Intra-animal comparisons of confocal AOSLO (A), transverse/horizontal TEM outer segment (OS) sections (B), and longitudinal/vertical TEM OS sections (C) before, during, and after hibernation. Photoreceptor schematic in (A) is based off of a model presented by (Jonnal et al., 2007), in which the confocal signal is thought to arise from the waveguiding properties of the photoreceptor; whereas the schematics in (B) and (C) show the photoreceptor plane visualized with TEM (dashed line). Disruptions in OS structure (red arrows) and abnormally enlarged structures (yellow arrow) may disrupt the normal waveguide properties of photoreceptors and affect their confocal AOSLO signal. AOSLO scale bar = 20 μm. TEM scale bars = 2 μm. (For interpretation of the references to colour in this figure legend, the reader is referred to the web version of this article.)

mitochondria) and 0.54 ± 0.35 μm^3 (3 cones, n = 402 mitochondria) in cones from euthermic and torpid 13-LGS, respectively; a significant increase in the volume of torpid mitochondria (P = < 0.0001, Mann-Whitney test; Fig. 6). The number of mitochondria in these cells was highly variable and not significantly different between the euthermic and torpid samples (P = 0.60, Kolmogorov-Smirnov test; Fig. 6A–C).

4. Discussion

The multiple physiological states of the 13-LGS seasonal cycle provide a natural model to investigate cellular adaptations to drastic metabolic fluctuations. Here, we report the non-invasive assessment of cone photoreceptor structural changes with cellular resolution AOSLO imaging during several distinct states of the seasonal cycle. We also provide intra-animal comparisons of cone structure with AOSLO imaging and TEM. To the best of our knowledge, this is this first attempt to examine structural changes of cones during hibernation with *in vivo* AOSLO imaging, and the first assessments of cone structure during intermediary states of the 13-LGS seasonal cycle (fall transition and IBE).

Kuwabara (1975) was the first to examine ground squirrel cones during hibernation. He observed shortening of cone outer segments without an increase in retinal pigment epithelium (RPE) phagosomes (Kuwabara, 1975). After two months of hibernation, cone outer segments were “almost absent in several animals” (Kuwabara, 1975), and cone structure fully recovered two weeks after hibernation. Two years later, Remé and Young (1977) described a more subtle shortening of cone outer segments, and also showed a reduction in the size and number of cone inner segment ellipsoid mitochondria. Mitochondrial size and number returned to euthermic levels 3 days after hibernation, while outer segment length followed suit 7 days after hibernation (Remé & Young, 1977).

Consistent with these reports, we demonstrate reversible cone degeneration during 13-LGS hibernation. Like Remé and Young and previous observations in our laboratory (Sajdak et al., 2018), we did not observe a complete disappearance of outer segments, but rather, highly variable disc remodeling (*e.g.* narrowed and clumped discs) within an intact cone sheath (Fig. 4C, Fig. 6). We find that this cone outer segment disc remodeling starts prior to the 13-LGS being introduced into a cold environment (Fig. 4). This transitional period between homeothermic and heterothermic physiology is often overlooked in hibernation studies. This period of fall transition occurs prior to cold exposure, where many 13-LGS undergo fall torpor bouts of varying length and frequency (Russell et al., 2010). We specifically selected animals that were in the fall transition torpid state (Fig. 1) and found disorganized outer segment disc structure (Fig. 4C), further evidence that 13-LGS cannot be considered “euthermic normal” during this period of fall transition (Russell et al., 2010).

Similar to Remé and Young (1977), our TEM analysis suggested reduced mitochondrial number in the torpid state (Fig. 5). However, when examining the entire mitochondrial structure in 3D using SEM, we found that mitochondria were increased in volume during torpor compared to euthermic 13-LGS (Fig. 6). An increase in mitochondrial volume in torpid 13-LGS conflicts with the current idea that “mitochondria are diminished in size” as seen with 2D TEM analysis (Remé & Young, 1977), and decreased volume in hibernating mitochondria (Kaden, Du, Goel, Lu, & Li, 2013; Li, Ball, & Chen, 2017). Our SEM data are limited to three cones each in one euthermic and one torpid 13-LGS. In addition, the SEM sectioning was done in different planes for the two samples (Fig. 6A–B), which could confound the 3D registration, manual segmentation, and resulting volume measurements seen. Together, our SEM data highlight a need for this type of 3D analysis to characterize changes at the level of individual cone photoreceptor mitochondria. More work is needed to define mitochondrial morphology in a population of euthermic 13-LGS, then assess how the morphology changes in each of the physiological states throughout the hibernation cycle (Fig. 1).

Using 2D TEM, the only significant increase in mitochondrial area relative to winter torpor was during IBE (Fig. 5). Surprisingly, not only

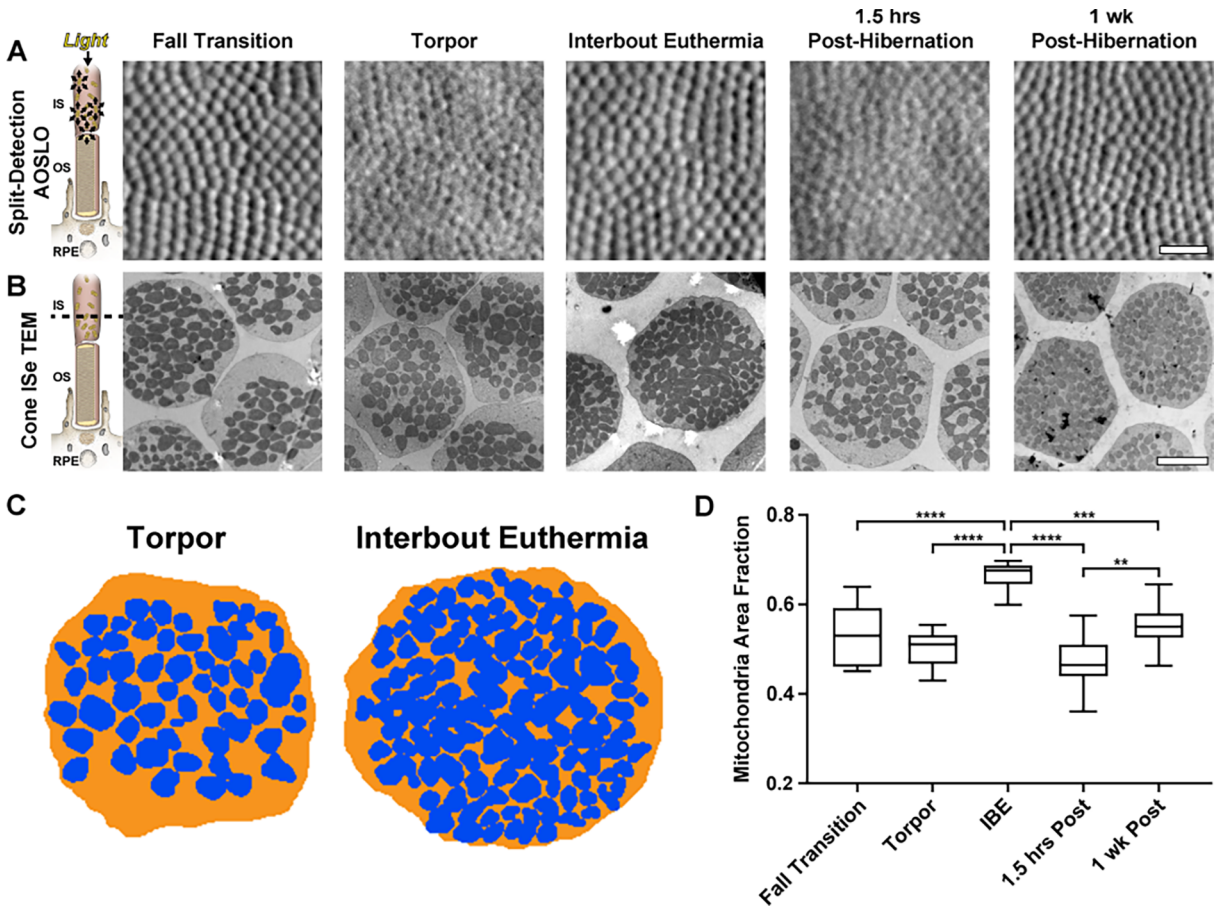

Fig. 5. Intra-animal comparisons of split-detection AOSLO (A) and transverse TEM inner segment ellipsoid (ISe) sections (B). Photoreceptor schematic in (A) illustrates the hypothesized sources of split-detection AOSLO signal (Scoles et al., 2014), whereas the schematic in (B) shows the photoreceptor plane visualized with TEM (dashed line). Photoreceptor mitochondria were sparser in fall transition, torpor, and 1.5 h post-hibernation, compared to interbout euthermia (IBE) and 1-week post-hibernation. Residual photoreceptor structure was detected in all seasonal states via split-detection AOSLO (A). Mitochondrial packing within the ISe does not have a noticeable effect on the split-detection AOSLO image (A & B). Representative torpor and IBE mitochondrial volume segmentations (blue) within the ISe (orange) are shown in (C). Box-and-whisker plots of mitochondria area fraction (mitochondria area ÷ ISe area) in 5 distinct physiological states are shown in (D). Boxes show median and interquartile ranges, *whiskers* show maximum and minimum values. IBE mitochondrial area fraction was significantly increased compared to all other physiological states, suggesting increased mitochondria recruitment during these brief periods of euthermia (D). $^{**}P < 0.01$; $^{***}P < 0.001$; $^{****}P < 0.0001$, one-way ANOVA. AOSLO scale bar = 20 μm. TEM scale bar = 2 μm. (For interpretation of the references to colour in this figure legend, the reader is referred to the web version of this article.)

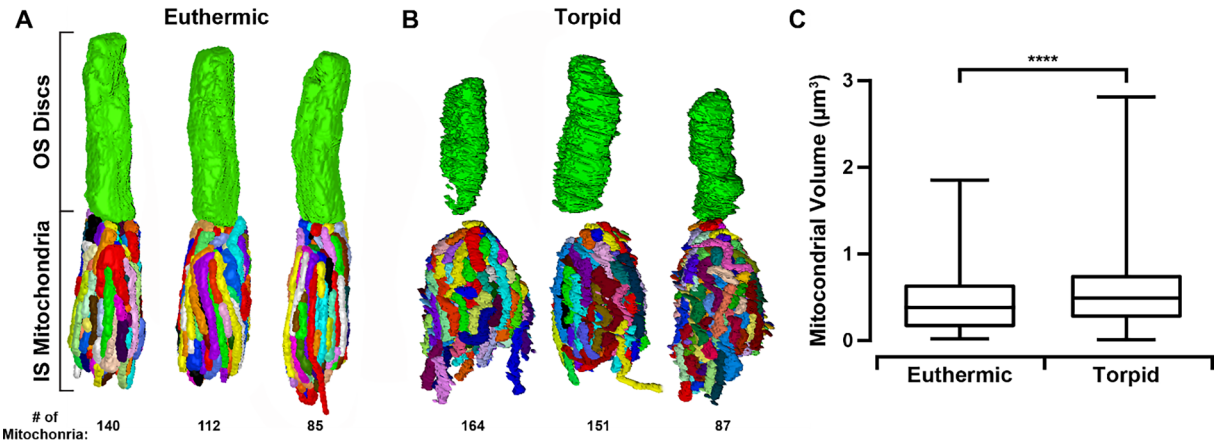

Fig. 6. 3D volume reconstructions of cones from euthermic (A) and torpid (B) 13-LGS. The euthermic 13-LGS was sectioned with photoreceptors aligned vertically (A), and the torpid 13-LGS retina was sectioned with photoreceptors aligned horizontally (B). (C) Box-and-whisker plots of mitochondrial volumes from the 6 cells in (A) and (B) show a significant increase in the volume of torpid mitochondria ($^{****}P < 0.0001$, Mann-Whitney test). *Boxes* show median and interquartile ranges, *whiskers* show maximum and minimum values.

was mitochondrial area higher during IBE compared to all other physiological states examined (Fig. 5C), but outer segment structure seemed to recover as well (Fig. 4C). IBE periods last about 12 to 24 h and occur every 1 to 2 weeks (e.g. Fig. 1, (Staples, 2016)). Since we tracked daily movement of each squirrel to determine if an IBE had occurred, our temporal data are limited to every 24 h. Therefore, while each IBE examined was of the expected rhythmicity relative to the previous IBE (1 to 2 weeks), we cannot know precisely when the IBE data were collected relative to its preceding torpor bout. Since the animals we examined during IBE had body temperatures of 35–37 °C, and the IBE time-course is well-established (Staples, 2016), we conservatively estimate IBE collection time-points were within a window of 2 to 24 h.

Given this window of time, it is somewhat surprising to find nearly complete recovery of the cone outer segment structure examined with AOSLO and TEM during states of IBE (Fig. 4). Cone outer segment renewal rate in euthermic mammals has been estimated to range from 1 to 2.7 μm/day (Jonnal et al., 2010; Long, Fisher, Fariss, & Anderson, 1986). Rod photoreceptor disc radiolabeling suggests a similar rate of outer segment renewal (frog: 1.5–3.8 μm/day (Besharse, Hollyfield, & Rayborn, 1977)). A complete renewal of an ~8 μm 13-LGS cone outer segment during these IBE states would thus require renewal rates more than twice as fast as these established rates. With an increased recruitment in mitochondria (Fig. 5C) and up to 88% of total ground squirrel energy throughout hibernation being used during IBEs (Staples, 2014; Wang & Wolowyk, 1988), it is conceivable that cone outer segments grow at an accelerated rate during this rapid shift in metabolic state. Alternatively, it is possible that the altered outer segment structure in torpid states makes this region more susceptible to variable disruption during histological processing. Alternative approaches such as cryoelectron tomography may limit potentially artefactual outer segment changes (Nickell, Park, Baumeister, & Palczewski, 2007). Our data warrant further investigation into this process of cone regeneration during IBE and post-hibernation physiological states, ideally with continuous monitoring of physiological states to more accurately detect transition periods. For example, electrocardiogram telemetry measurements of heart rate was found to be more sensitive at detecting IBE compared to measuring body temperature (MacCannell, Jackson, Mathers, & Staples, 2018). Since torpid and IBE states are experienced in complete darkness, we expect a minimal influence from a typical light–dark shedding cycle. Indeed, previous hibernation studies suggest that circadian rhythms are inhibited during hibernation (Revel et al., 2007; Williams, Barnes, Richter, & Buck, 2012), but the extent to which photoreceptor disc shedding cycles change during hibernation is not known.

Overall, the 13-LGS cone mosaic is unaffected by the hibernation cycle (Figs. 2 and 3), meaning that cones do not degenerate completely, but that intact outer segment sheaths and inner segments remain in an unperturbed mosaic despite the changes to subcellular structures within (i.e. outer segment discs and inner segment mitochondria). The rare cone that becomes undetectable into the summer months (Fig. 3) likely represents no consequence to a squirrel's vision, given that visual acuity in humans is not abnormal until cone density is 38–62% below normal (Ratnam, Carroll, Porco, Duncan, & Roorda, 2013; Sun et al., 2016). These voids seem to persist in the mosaic, as no cell migration into these spaces was observed. This suggests that either these cones are altered in a way that affects their AOSLO detection properties, or that the cone outer segments and inner segments have degenerated. The former scenario may be more likely, given that rods expand to fill vacant photoreceptor space in humans (Curcio, Millican, Allen, & Kalina, 1993; Hansen, Cooper, Dubra, Carroll, & Weinberg, 2013). However, it is not known if this kind of photoreceptor migration occurs in cone-dominated mosaics.

Photoreceptor structure visualized with split-detection AOSLO imaging is thought to arise from the photoreceptor inner segment due to its similarity to the appearance and diameter of inner segments visualized with Nomarski differential interference contrast imaging (Scoles et al., 2014). Non-reflective cones are thought to have absent or altered outer segments, which affects confocal AOSLO signal but not multiply-scattered light detected with non-confocal AOSLO (e.g. split-detection AOSLO) (Langlo et al., 2017; Sun et al., 2016). However, little is known about how/if mitochondria are involved in these signals. Our results indicate that any changes in inner segment mitochondria occurring during hibernation do not prevent visualization of inner segments by split-detection AOSLO (Figs. 2, 3, and 5). Image quality of split-detection images was reduced during torpor and 1.5 h post-hibernation imaging (Figs. 3 and 5A), but cells were still detectable during these and all other physiological states examined. Changes to the anterior segment, like corneal stroma thickening during torpor (Sajdak et al., 2018), likely diminish AOSLO image quality during torpor.

Cone reflectance detected with confocal AOSLO is thought to arise from the concomitant waveguiding properties of the cone (Jonnal et al., 2007; Scoles et al., 2014). We reasoned that outer segment disruption during hibernation would affect the waveguiding properties of the cones and alter confocal AOSLO signal. Indeed, confocal AOSLO images of the cone mosaic were disrupted when examining 13-LGSs in fall transition torpor, winter torpor, and 1.5 h post-hibernation (arousal to euthermia), compared to IBE, 24 h post-hibernation, and thereafter (Figs. 3 and 4). Considering the intra-animal structural changes in outer segment discs seen with TEM and AOSLO at the same retinal regions, we conclude that intact outer segments are not required to visualize inner segments with split-detection AOSLO. This was suspected based on the initial observations in patients with achromatopsia (Scoles et al., 2014) in whom histological validation was not possible. These *in vivo* to *ex vivo* comparisons have scaling limitations, in that axial length was not measured in the animals and therefore scale is approximated by degrees, or microns using an assumed axial length of 7.9 mm (axial length of the European ground squirrel (Hughes, 1977).

Recent reports suggest that such "dysflective" cones can be functional despite the absence of reflective properties detectable with confocal AOSLO (Bruce et al., 2015; Tu et al., 2017; Wang et al., 2015). Future work should assess *in vivo* cone function by measuring responses to light stimuli (Cooper, Tuten, Dubra, Brainard, & Morgan, 2017) to examine what degree of structure is required for cone function and how rapidly cone function recovers following hibernation.

Acknowledgements

The authors thank Tiffany Butler, Lisa King, Christine Skumatz, Joseph Thulin, and the Biomedical Resource Center at MCW for their contributions to ground squirrel care, Rob Goodwin for help preparing TEM samples, Emily Benson and Grahame Kidd for preparing and imaging the SEM samples, Rob Cooper for developing and supporting custom software for image analysis, and Joseph Besharse for the helpful discussions related to EM interpretation.

Disclosures

B.S. Sajdak, none; A.E. Salmon, none; D.K. Merriman, none; K.M. Litts, none; C. Wells, none; K.P. Allen, none; A. Dubra, none; J. Carroll, none.

Grant information

Research in the manuscript was supported by the National Eye Institute of the National Institutes of Health (NIH) under award numbers P30EY001931, T32EY014537, U01EY025477, and U24EY029891. This investigation was conducted in a facility constructed with support from Research Facilities Improvement Program Grant Number C06RR016511 from the National Center for Research Resources, NIH. The content is solely the responsibility of the authors and does not necessarily represent the official views of the NIH. Additional support

from the Foundation Fighting Blindness consortium PPA-0641-0718-UCSF, an unrestricted departmental grant from Research to Prevent Blindness, the Alcon Research Institute, and the Gene & Ruth Posner Foundation.

References

Andrews, M. T. (2007). Advances in molecular biology of hibernation in mammals. *BioEssays, 29*, 431–440. https://doi.org/10.1002/bies.20560.

Besharse, J. C., Hollyfield, J. G., & Rayborn, M. E. (1977). Turnover of rod photoreceptor outer segments. II. Membrane addition and loss in relationship to light. *Journal of Cell Biology, 75*, 507–527.

Bruce, K. S., Harmening, W. M., Langston, B. R., Tuten, W. S., Roorda, A., & Sincich, L. C. (2015). Normal perceptual sensitivity arising from weakly reflective cone photoreceptors. *Investigative Ophthalmology and Visual Science, 56*, 4431–4438. https://doi.org/10.1167/iovs.15-16547.

Cardona, A., Saalfeld, S., Schindelin, J., Arganda-Carreras, I., Preibisch, S., Longair, M., ... Douglas, R. J. (2012). TrakEM2 software for neural circuit reconstruction. *PLoS One, 7*, e38011. https://doi.org/10.1371/journal.pone.0038011.

Carey, H. V., Andrews, M. T., & Martin, S. L. (2003). Mammalian hibernation: Cellular and molecular responses to depressed metabolism and low temperature. *Physiological Reviews, 83*, 1153–1181.

Carroll, J., Choi, S. S., & Williams, D. R. (2008). In vivo imaging of the photoreceptor mosaic of a rod monochromat. *Vision Research, 48*, 2564–2568. https://doi.org/10.1016/j.visres.2008.04.006.

Chen, M., Cooper, R. F., Han, G. K., Gee, J., Brainard, D. H., & Morgan, J. I. (2016). Multimodal automatic montaging of adaptive optics retinal images. *Biomedical Optics Express, 7*, 4899–4918. https://doi.org/10.1364/BOE.7.004899.

Christian, S. L., Rasley, B. T., Roe, T., Moore, J. T., Harris, M. B., & Drew, K. L. (2014). Habituation of Arctic ground squirrels (Urocitellus parryii) to handling and movement during torpor to prevent artificial arousal. *Frontiers in Physiology, 9*. https://doi.org/10.3389/fphys.2014.00174.

Cooper, S. T., Sell, S. S., Fahrenkrog, M., Wilkinson, K., Howard, D. R., Bergen, H., ... Hampton, M. (2016). Effects of hibernation on bone marrow transcriptome in thirteen-lined ground squirrels. *Physiological Genomics, 48*, 513–525. https://doi.org/10.1152/physiolgenomics.00120.2015.

Cooper, R. F., Tuten, W. S., Dubra, A., Brainard, D. H., & Morgan, J. I. W. (2017). Noninvasive assessment of human cone photoreceptor function. *Biomedical Optics Express, 8*, 5098–12112. https://doi.org/10.1364/BOE.8.005098.

Cooper, R. F., Wilk, M. A., Tarima, S., & Carroll, J. (2016). Evaluating descriptive metrics of the human cone mosaic. *Investigative Ophthalmology and Visual Science, 57*, 2992–3001. https://doi.org/10.1167/iovs.16-19072.

Cunefare, D., Cooper, R. F., Higgins, B., Katz, D. F., Dubra, A., Carroll, J., & Farsiu, S. (2016). Automatic detection of cone photoreceptors in split detector adaptive optics scanning light ophthalmoscope images. *Biomedical Optics Express, 7*, 2036–2050. https://doi.org/10.1364/BOE.7.002036.

Curcio, C. A., Millican, C. L., Allen, K. A., & Kalina, R. E. (1993). Aging of the human photoreceptor mosaic: Evidence for selective vulnerability of rods in central retina. *Investigative Ophthalmology and Visual Science, 34*, 3278–3296.

Deerinck, T. J., Bushong, E. A., Lev-Ram, V., Shu, X., Tsien, R. Y., & Ellisman, M. H. (2010). Enhancing serial block-face scanning electron microscopy to enable high resolution 3-D nanohistology of cells and tissues. *Microscopy and Microanalysis, 16*, 1138–1139.

Dubra, A., & Harvey, Z. (2010). Registration of 2D images from fast scanning ophthalmic instruments. In B. Fischer, B. Dawant, & C. Lorenz (Eds.). *Biomedical Image Registration* (pp. 60–71). (1 ed.). Berlin: Springer-Verlag.

Dubra, A., & Sulai, Y. (2011). Reflective afocal broadband adaptive optics scanning ophthalmoscope. *Biomedical Optics Express, 2*, 1757–1768.

Hansen, S. O., Cooper, R. F., Dubra, A., Carroll, J., & Weinberg, D. V. (2013). Selective cone photoreceptor injury in acute macular neuroretinopathy. *Retina, 33*, 1650–1658. https://doi.org/10.1097/IAE.0b013e31828cd03a.

Horton, J. C., Parker, A. B., Botelho, J. V., & Duncan, J. L. (2015). Spontaneous regeneration of human photoreceptor outer segments. *Scientific Reports, 5*. https://doi.org/10.1038/srep12364.

Hughes, A. (1977). The topography of vision in animals with contrasting life styles. In F. Crescitelli (Ed.). *Handbook of sensory physiology* (pp. 614–642). Berlin: Springer.

Jagger, W. S. (1985). Visibility of photoreceptors in the intact living cane toad eye. *Vision Research, 25*, 729–731.

Jonnal, R. S., Besecker, J. R., Derby, J. C., Kocaoglu, O. P., Cense, B., Gao, W., ... Miller, D. T. (2010). Imaging outer segment renewal in living human cone photoreceptors. *Optics Express, 18*, 5257–5270. https://doi.org/10.1364/OE.18.005257.

Jonnal, R. S., Rha, J., Zhang, Y., Cense, B., Gao, W., & Miller, D. T. (2007). In vivo functional imaging of human cone photoreceptors. *Optics Express, 14*, 16141–16160.

Kaden, T., Du, J., Goel, A., Lu, G., & Li, W. (2013). Structural and functional properties of photoreceptor mitochondria in awake and hibernating ground squirrels. E-abstract: 6082 *Investigative Ophthalmology and Visual Science, 54*.

Kryger, Z., Galli-Resta, L., Jacobs, G. H., & Reese, B. E. (1998). The topography of rod and cone photoreceptors in the retina of the ground squirrel. *Visual Neuroscience, 15*, 685–691.

Kuwabara, T. (1975). Cytologic changes of the retina and pigment epithelium during hibernation. *Investigative Ophthalmology, 14*, 457–467.

Land, M. F., & Snyder, A. W. (1985). Cone mosaic observed directly through natural pupil of live vertebrate. *Vision Research, 25*, 1519–1523.

Langlo, C. S., Erker, L. R., Parker, M., Patterson, E. J., Higgins, B. P., Summerfelt, P., Razeen, M. M., Collison, F. T., Fishman, G. A., Kay, C. N., Zhang, J., Weleber, R. G., Yang, P., Pennesi, M. E., Lam, B. L., Chulay, J. D., Dubra, A., Hauswirth, W. W., Wilson, D. J., & Carroll, J. (2017). ACHM-001 Study Group, 2017. Repeatability and longitudinal assessment of foveal cone structure in *CNGB3*-associated achromatopsia. *Retina,* 1956–1966. https://doi.org/10.1097/IAE.0000000000001434.

Li, W., Ball, J., & Chen, S. (2017). Cone mitochondria enhance light transmission. E-Abstract: 1037 *Investigative Ophthalmology and Visual Science, 58*.

Long, K. O., Fisher, S. K., Fariss, R. N., & Anderson, D. H. (1986). Disc shedding and autophagy in the cone-dominant ground squirrel retina. *Experimental Eye Research, 43*, 193–205.

MacCannell, A. D. V., Jackson, E. C., Mathers, K. E., & Staples, J. F. (2018). An improved method for detecting torpor entrance and arousal in a mammalian hibernator using heart rate data. *Journal of Experimental Biology, 221*, jeb174508. https://doi.org/10.1242/jeb.174508.

Merriman, D. K., Lahvis, G., Jooss, M., Gesicki, J. A., & Schill, K. (2012). Current practices in a captive breeding colony of 13-lined ground squirrels (*Ictidomys tridecemlineatus*). *Lab Animal, 41*, 315–325. https://doi.org/10.1038/laban.150.

Merriman, D. K., Sajdak, B. S., Li, W., & Jones, B. W. (2016). Seasonal and post-trauma remodeling in cone-dominant ground squirrel retina. *Experimental Eye Research, 150*, 90–105. https://doi.org/10.1016/j.exer.2016.01.011.

Miller, D. T., Williams, D. R., Morris, G. M., & Liang, J. (1996). Images of cone photoreceptors in the living human eye. *Vision Research, 36*, 1067–1079.

Mukherjee, R., Clark, H. R., Chavan, V., Benson, E. K., Kidd, G. J., & Srivastava, S. (2016). Analysis of brain mitochondria using serial block-face scanning electron microscopy. *Journal of Visualized Experiments*. https://doi.org/10.3791/54214.

Nickell, S., Park, P. S., Baumeister, W., & Palczewski, K. (2007). Three-dimensional architecture of murine rod outer segments determined by cryoelectron tomography. *Journal of Cell Biology, 177*, 917–925. https://doi.org/10.1083/jcb.200612010.

Pallikaris, A., Williams, D. R., & Hofer, H. (2003). The reflectance of single cones in the living human eye. *Investigative Ophthalmology and Visual Science, 44*, 4580–4592.

Pengelley, E. T., & Fisher, K. C. (1961). Rhythmical arousal from hibernation in the golden-mantled ground squirrel, *Citellus lateralis tescorum*. *Canadian Journal of Zoology, 39*, 105–120.

Ratnam, K., Carroll, J., Porco, T. C., Duncan, J. L., & Roorda, A. (2013). Relationship between foveal cone structure and clinical measures of visual function in patients with inherited retinal degenerations. *Investigative Ophthalmology and Visual Science, 54*, 5836–5847. https://doi.org/10.1167/iovs.13-12557.

Remé, C. E., & Young, R. W. (1977). The effects of hibernation on cone visual cells in the ground squirrel. *Investigative Ophthalmology and Visual Science, 16*, 815–840.

Revel, F. G., Herwig, A., Garidou, M. L., Dardente, H., Menet, J. S., Masson-Pevet, M., ... Pevet, P. (2007). The circadian clock stops ticking during deep hibernation in the European hamster. *Proceedings of the National Academy of Sciences of the United States of America, 104*, 13816–13820.

Roorda, A., & Duncan, J. L. (2015). Adaptive optics ophthalmoscopy. *Annual Review of Vision Science, 1*, 19–50. https://doi.org/10.1146/annurev-vision-082114-035357.

Roorda, A., Romero-Borja, F., Donnelly, W. J., 3rd, Queener, H., Hebert, T., & Campbell, M. (2002). Adaptive optics scanning laser ophthalmoscopy. *Optics Express, 10*, 405–412.

Russell, R. L., O'Neill, P. H., Epperson, L. E., & Martin, S. L. (2010). Extensive use of torpor in 13-lined ground squirrels in the fall prior to cold exposure. *Journal of Comparative Physiology B, 180*, 1165–1172. https://doi.org/10.1007/s00360-010-0484-8.

Sajdak, B. S., Bell, B. A., Lewis, T. R., Luna, G., Cornwell, G. S., Fisher, S. K., ... Carroll, J. (2018). Assessment of outer retinal remodeling in the hibernating 13-lined ground squirrel. *Investigative Ophthalmology and Visual Science, 59*, 2538–2547.

Sajdak, B., Sulai, Y. N., Langlo, C. S., Luna, G., Fisher, S. K., Merriman, D. K., & Dubra, A. (2016). Noninvasive imaging of the thirteen-lined ground squirrel photoreceptor mosaic. *Visual Neuroscience, 33*, e003. https://doi.org/10.1017/S0952523815000346.

Salmon, A. E., Cooper, R. F., Langlo, C. S., Baghaie, A., Dubra, A., & Carroll, J. (2017). An automated reference frame selection (ARFS) algorithm for cone imaging with adaptive optics scanning light ophthalmoscopy. *Translational Vision Science and Technology, 6*, 9. https://doi.org/10.1167/tvst.6.2.9.

Schindelin, J., Arganda-Carreras, I., Frise, E., Kaynig, V., Longair, M., Pietzsch, T., ... Cardona, A. (2012). Fiji: An open-source platform for biological-image analysis. *Nature Methods, 9*, 676–682. https://doi.org/10.1038/nmeth.2019.

Scoles, D., Sulai, Y. N., & Dubra, A. (2013). In vivo dark-field imaging of the retinal pigment epithelium cell mosaic. *Biomedical Optics Express, 4*, 1710–1723. https://doi.org/10.1364/BOE.4.001710.

Scoles, D., Sulai, Y. N., Langlo, C. S., Fishman, G. A., Curcio, C. A., Carroll, J., & Dubra, A. (2014). In vivo imaging of human cone photoreceptor inner segments. *Investigative Ophthalmology and Visual Science, 55*, 4244–4251. https://doi.org/10.1167/iovs.14-14542.

Song, H., Rossi, E. A., Latchney, L., Bessette, A., Stone, E., Hunter, J. J., ... Chung, M. (2015). Cone and rod loss in Stargardt disease revealed by adaptive optics scanning light ophthalmoscopy. *JAMA Ophthalmology, 133*, 1198–1203. https://doi.org/10.1001/jamaophthalmol.2015.2443.

Staples, J. F. (2014). Metabolic suppression in mammalian hibernation: The role of mitochondria. *Journal of Experimental Biology, 217*, 2032–2036. https://doi.org/10.1242/jeb.092973.

Staples, J. F. (2016). Metabolic flexibility: Hibernation, torpor, and estivation. *Comprehensive Physiology, 6*, 737–771. https://doi.org/10.1002/cphy.c140064.

Sun, L. W., Johnson, R. D., Langlo, C. S., Cooper, R. F., Razeen, M. M., Russillo, M. C., ... Carroll, J. (2016). Assessing photoreceptor structure in retinitis pigmentosa and Usher syndrome. *Investigative Ophthalmology and Visual Science, 57*, 2428–2442. https://doi.org/10.1167/iovs.15-18246.

Tu, J. H., Foote, K. G., Lujan, B. J., Ratnam, K., Qin, J., Gorin, M. B., ... Roorda, A. (2017). Dysflective cones: Visual function and cone reflectivity in long-term follow-up of acute bilateral foveolitis. *American Journal of Ophthalmology Case Reports, 7*, 14–19. https://doi.org/10.1016/j.ajoc.2017.04.001.

Vermillion, K. L., Jagtap, P., Johnson, J. E., Griffin, T. J., & Andrews, M. T. (2015). Characterizing cardiac molecular mechanisms of mammalian hibernation via quantitative proteogenomics. *Journal of Proteome Research, 14*, 4792–4804. https://doi.org/10.1021/acs.jproteome.5b00575.

von Schantz, M., Szél, A., van Veen, T., & Farber, D. B. (1994). Expression of phototransduction cascade genes in the ground squirrel retina. *Investigative Ophthalmology and Visual Science, 35*, 2558–2566.

Wade, A. R., & Fitzke, F. W. (1998). In vivo imaging of the human cone-photoreceptor mosaic using a confocal laser scanning ophthalmoscope. *Lasers and Light in Ophthalmology, 8*, 129–136.

Wang, Q., Tuten, W. S., Lujan, B. J., Holland, J., Bernstein, P. S., Schwartz, S. D., ... Roorda, A. (2015). Adaptive optics microperimetry and OCT images show preserved function and recovery of cone visibility in macular telangiectasia type 2 retinal lesions. *Investigative Ophthalmology and Visual Science, 56*, 778–786. https://doi.org/10.1167/iovs.14-15576.

Wang, L. C. H., & Wolowyk, M. W. (1988). Torpor in mammals and birds. *Canadian Journal of Zoology, 66*, 133–137.

Williams, C. T., Barnes, B. M., Richter, M., & Buck, C. L. (2012). Hibernation and circadian rhythms of body temperature in free-living Arctic ground squirrels. *Physiological and Biochemical Zoology, 85*, 397–404.